Kinetics of structural changes in superhelical DNA

Gero Wedemann, Christian Münkel,* Gunther Schöppe,† and Jörg Langowski‡
Biophysics of Macromolecules (H0500), German Cancer Research Center (DKFZ), Im Neuenheimer Feld 280, 69120 Heidelberg and Interdisciplinary Center for Scientific Computing, University of Heidelberg, Im Neuenheimer Feld 368, 69120 Heidelberg, Germany
(Received 24 July 1997; revised manuscript received 30 March 1998)

The time evolution of global structural rearrangements in supercoiled DNA caused by changes in local bending was investigated using Brownian dynamics computer simulations. Equilibrium states of superhelical DNA with lengths from 1180 to 1770 base pairs were modeled at different values of the linking number and in different ionic strength solutions. The introduction of a local bend induces a transition to a new equilibrium state where one end loop of the plectonemic structure is at the position of the permanent bend. This transition occurs on a time scale of 1 ms. We find that the transition can proceed either by a ''reptational motion'' of the two opposing double strands (slithering) or by extrusion/absorption of branched parts of the superhelix. We estimate the diffusion coefficient for the motion of the two double strands against each other. A simplified model for this kinetics based on a transition matrix is presented. The relaxation time scales approximately with the square of the DNA length. [S1063-651X(98)06809-3]

PACS number(s): 87.15.Da, 05.40.+j, 87.15.He

I. INTRODUCTION

An important step in the activation of transcription is the interaction of a transcription factor bound to an enhancer site with the transcription complex bound to the promoter. Enhancer and promoter may be hundreds or thousands of base pairs apart, too far for a direct interaction, which therefore proceeds through the formation of a DNA loop. The probability of forming this loop can depend on the structure of the intervening DNA. It has been argued, for instance, that bends induced by other DNA-binding proteins or by specific sequences can help form the loop by bringing the ends of the DNA segment into contact [1–4].

For distances up to about 500 base pairs (bp) this increase of contact probability is mainly a direct consequence of the bending of the DNA segment. At longer distances, the end-to-end distance of a linear DNA is not influenced much by the presence of internal bends; however, it could be shown experimentally [5,6] and theoretically [7] that in a superhelical DNA bends localize with preference in the end loops of the interwound structure. This localization will greatly enhance the interaction probability of DNA sites that are located symmetrically with respect to the bend. Thus, upon insertion of a bend into the plectonemic region of a superhelix, the structure will globally rearrange so that an end loop is formed at the position of the bend. While the principal phenomenon has been known for some time, the kinetics of structural rearrangements after local bending (e.g., due to interaction with regulatory proteins) has not been studied in great detail. We have recently given indications that bend-induced conformational transitions in superhelical DNA are comparatively slow; for a structural transition induced by placing a bend in the center of an 1870-bp interwound superhelix, the characteristic time for forming the new end loop was 0.5 ms [8].

In order to assess the time scales on which such global structural transitions in superhelical DNA occur and to determine their mechanisms, it now becomes important to investigate systematically the dependence of their kinetics on parameters such as DNA length, superhelical density, or ionic strength. While a variety of techniques have been used to model the global structure and dynamics of DNA [9], the major part of such studies focused on analyzing equilibrium properties of superhelical DNA such as the ratio of twist to writhe, radius of gyration, or diffusion coefficients. Brownian dynamics (BD) [10] offers the unique advantage that, unlike other models [11,12], it does not need arbitrary constants or rescaling of energy in order to get the correct time evolution of a polymer chain in a viscous medium. Only such parameters are used that are accessible by means of physical measurements such as flexibility of the DNA, charge density, hydrodynamic, and electrostatic radius.

The results of the present article are based on BD-simulated trajectories of (1180–1770)-bp superhelical DNA at varying linking numbers in aqueous solution for a total simulation time of 400 ms. We obtain information on the equilibrium dynamics as well as the kinetics of structural rearrangement after inserting a 90° permanent bend.

II. METHODS

A. Brownian dynamics algorithm

Our BD model is based on the algorithm proposed by Ermak and McCammon [10] and Fixman [13]. Similar models have been applied to DNA for some time (e.g., [14] and later work by the same author). We have recently extended the BD algorithm to include the topological constraints of superhelical DNA and local bending [8,15,4].

*Present address: SAP AG, Neurottstrasse 16, 69090 Walldorf, Germany.
†Institut für Theoretische Physik, University of Heidelberg, Abt. Vielteilchenphysik, Philosopherweg 19, 69120 Heidelberg, Germany.
‡Author to whom correspondence should be addressed. Electronic address: Joerg.Langowski@DKFZ-Heidelberg.de

In this work we used the program CORCHY written by Klenin *et al.* as described in detail in [4]. The DNA is described as a chain of beads. A local coordinate system is attached to each bead. The coordinate system at bead i can be transformed to the coordinate system at bead $i+1$ by a Euler transformation with the angles α_i, β_i, and γ_i. The distance between two adjacent beads is much smaller than the persistence length (about 5 times). The beads interact through elastic forces. The energies for stretching $U^{(s)}$, bending $U^{(b)}$, and torsion $U^{(t)}$ can be computed as

$$U^{(s)}(b_i)=\alpha^{(s)}\frac{k_bT}{2}(b_i-b_i^0)^2,$$

$$U^{(b)}(\beta_i)=\alpha^{(b)}\frac{k_bT}{2}\beta_i^2,$$

$$U^{(t)}(\alpha_i+\gamma_i)=\alpha^{(t)}\frac{k_bT}{2}(\alpha_i+\gamma_i)^2. \tag{1}$$

The electrostatic interaction between the charged phosphate backbone is described by a solution of the Debye-Hückel equation for two charged line segments

$$E_{ij}^{(e)}=\frac{\nu^2}{D}\int d\lambda_i\int d\lambda_j\frac{\exp(-\kappa r_{ij})}{r_{ij}}. \tag{2}$$

D is the dielectric constant of water and κ the inverse of the Debye length. r_{ij} is the distance between the current positions at the segments to which the integration parameters λ_i,λ_j correspond. The charge per unit length ν is chosen such that the potential at the radius of the DNA coincides with the solution of the Poisson-Boltzmann equation for a cylinder with charge per length ν_0^*. ν_0^* is the charge per length of the DNA in the presence of the Gouy layer of immobile counterions, which can be computed as [16]

$$\nu_0^*=q\nu_0, \tag{3}$$

where $\nu_0=-2e/\Delta$ is the charge per length of the naked DNA. e is the proton charge and $\Delta=0.34$ nm is the distance between base pairs. Following Stigter [16], the value of q is 0.73. In order to save computation time a tabulation of the the double integral (2) is used. The table is parametrized by the distance of the segments and three values describing its relative orientation. During the simulation a linear interpolation was used to obtain the forces.

Bent sequences are realized using a vector B_i describing the equilibrium position of one segment with respect to its neighbor segment [4]. The energy of bending changes then to

$$U^{(b)}(\theta_i)=\alpha^{(b)}\frac{k_bT}{2}\theta_i^2, \tag{4}$$

where θ_i is defined by $\cos(\theta_i)=\vec{B}_i\cdot\vec{u}_{i+1}$ with the vector u_i pointing from bead i to bead $i+1$. Hydrodynamic interactions are treated using the Rotne-Prager tensor [17]

TABLE I. Parameters used in the simulation.

Stretching persistence length	308 nm
Bending persistence length	50 nm
Torsion persistence length	65 nm
Hydrodynamic radius	1.2 nm
Electrostatic radius	1.2 nm
Temperature	20 °C
Length of segments	10 nm
Time step of simulation	20 ns

$$D_{ij}=\delta_{ij}\frac{k_bT}{6\pi\eta\sigma}-(\delta_{ij}-1)\frac{k_bT}{8\pi\eta r_{ij}}\times\left[\left(1+\frac{\vec{r}_{ij}\cdot\vec{r}_{ij}}{r_{ij}^2}\right)+\frac{2\sigma^2}{r_{ij}^2}\left(\frac{1}{3}-\frac{\vec{r}_{ij}\cdot\vec{r}_{ij}}{r_{ij}^2}\right)\right]. \tag{5}$$

Starting from one configuration, the next configuration is generated by a first-order displacement of the position vectors $\vec{r}_i$ and the relative twisting angles $\vec{\phi}_i$:

$$\vec{r}_i(t+\delta t)=\vec{r}_i(t)+\sum_{j=1}^{N}D_{ij}\vec{F}_j\frac{\delta t}{k_bT}+\vec{R}_i(t),$$
$$\vec{\phi}_i(t+\delta t)=\vec{\phi}_i(t)+D_rT_i\frac{\delta t}{k_bT}+g_i(t)R_i(t), \tag{6}$$

where N is the number of segments, F_i the sum of the acting forces, D_r the rotational diffusion coefficient of a segment, and T_i the acting torque. The random displacements R_i and g_i are Gaussian distributed and have the properties

$$\langle\vec{R}_i(t)\rangle=\vec{0},\quad\langle\vec{R}_i(t)\cdot\vec{R}_j(t)\rangle=2D_{ij}\delta t,$$
$$\langle g_i(t)\rangle=\vec{0},\quad\langle g_i(t)g_j(t)\rangle=2D_r\delta_{ij}\delta t. \tag{7}$$

We used commonly accepted values for the parameters (Table I). During the course of this work a value of 66 nm for the stretching persistence length was published [18], which is different from the one used here. However, as reported by Hammermann [19], the quantities simulated here are not influenced much by a change in stretching constant.

All simulations started initially from a flat circle. The measurement started after full relaxation of the system, which took about 1–2 ms corresponding to the slowly decaying component of the relaxation of the writhe [8].

B. Characterization of the structure

1. End loop detection

The global structure and dynamics of a plectonemic superhelix can be described by a plot of the end loop positions versus time [20]. While we and others have described several algorithms for automatic end loop detection [7,8,20], we found their detection efficiency not always satisfactory. We therefore developed an improved algorithm (Appendix), which we tested by comparing the automatically detected end loop positions in 150 random configurations with their visualizations. All end loops determined by the algorithm

were also found by visual inspection without any false positives; about 10% of the loops were false negatives, i.e., the algorithm could not find them, although they were present in the visualization.

2. Superhelix diameter

The nearest neighbor $n_{nb}(i)$ of a segment i is defined as the segment with the shortest distance to i excluding a number of adjacent segments equal to the number of segments in an end loop (eight in our case). The superhelix diameter d_{SH} is calculated as the mean value of the distance of each segment to its nearest neighbor [21]:

$$d_{SH}=\overline{|\vec{x}_i(t)-\vec{x}_{n_{nb}(i)}(t)|}. \tag{8}$$

In contrast to the original definition, we omitted the segments in the end loops because they do not belong to the plectonemic region(s) by skipping the four segments that are adjacent to the segment detected as an end loop.

3. Diffusion coefficient

The random movement of a point in N-dimensional space can be described by a random walk. The mean square of the displacement $x(t)$ of the point after a time t is

$$\langle x^2\rangle = 2NDt. \tag{9}$$

The random movement of both strands of a plectonemic structure against each other (slithering) can be described as a one-dimensional random walk. We can calculate a diffusion coefficient for this motion through the change in the end loop position. The random displacement x is calculated using the difference between the position of one end loop of the considered configuration and that of the start configuration after the time t. For a one-dimensional random walk with diffusion coefficient D_{sl} the mean square displacement $\langle x^2\rangle$ is, according to Eq. (9),

$$\langle x^2\rangle = 2D_{sl}t. \tag{10}$$

A plot of $D_{sl}(t)=\langle x^2\rangle/2t$ versus t will yield the dependence of D_{sl} on the time scale.

III. RESULTS

A. Equilibrium

In order to check the hydrodynamics of CORCHY we performed simulations of a 50-nm linear DNA fragment at $I=0.1M$ NaCl for 40 ms. Figure 1 shows the mean of the squared displacement of the center of mass at a time difference t vs t. A fit of Eq. (9) to the first 15 ms results in a diffusion coefficient of $(2.85\pm 0.01)\times 10^{-11}$ m^2/s.

Brownian dynamics calculations on a superhelical DNA were done for each set of parameters for 5–20 ms. Figure 2 shows the end loop plot of a 1475-bp DNA structure (50 segments) at $\Delta Lk=-8$ and an ionic strength of $0.1M$ NaCl. After the first millisecond the DNA has two end loops and the writhe has reached its equilibrium value (data not shown). Most of the time we find two end loops with a distance of about 50% of the total length, indicating the absence of branches. For a total time of about 2.2 ms, three-looped branched configurations are observed. It is equivalent to a fraction of branched states of $2.2/19\approx 0.12$. This is an approximate value because the trajectory is too short for an exact determination of this value: Here we observed only one short time period of three arm configurations.

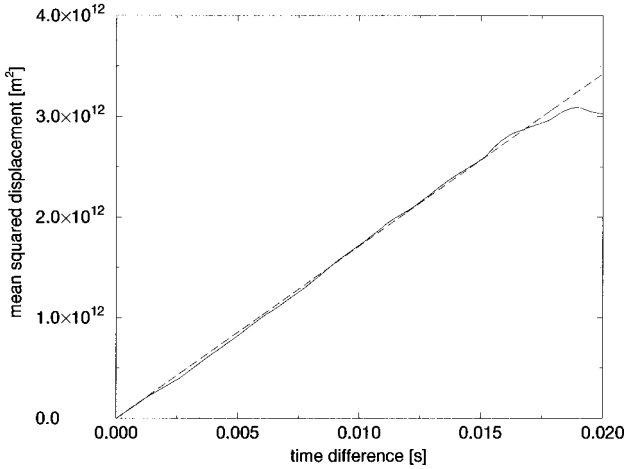

FIG. 1. Mean of the squared displacement of the center of mass at a time difference t vs t of a 50-nm linear DNA structure at $0.1M$ NaCl and a linear fit of the first 15 ms (dashed line).

The apparent slithering diffusion coefficient of this system $D_{sl}=\langle x^2\rangle/2t$ is plotted against t in Fig. 3. It decreases with t, indicating the predominance of faster local motion on short time scales. The initial value of D_{sl} is 31.7×10^{-12} m^2/s. D_{sl} approaches a plateau for large t. The statistical noise for values greater than 0.4 ms on D_{sl} becomes rather high so that the plateau value is better determined from an extrapolation of D_{sl} versus $1/t$ to $t\to\infty$ (Fig. 4). The plateau value of D_{sl} is $(2.5\pm 0.2)\times 10^{-12}$ m^2/s.

The dynamics of the DNA changes if we introduce a permanent bend in the chain. Figure 5 is an end loop plot of the same superhelical DNA as above but with a permanent bend at position 0. Almost always the end loops are located around 0% and 50% of the length of the DNA. We observe three arm branched configurations in the intervals [6.5 ms, 7.8 ms], [10.9 ms, 13.4 ms], and [14.4 ms, 16.3 ms]. Skipping the first 1.5 ms we compute an approximate ratio of

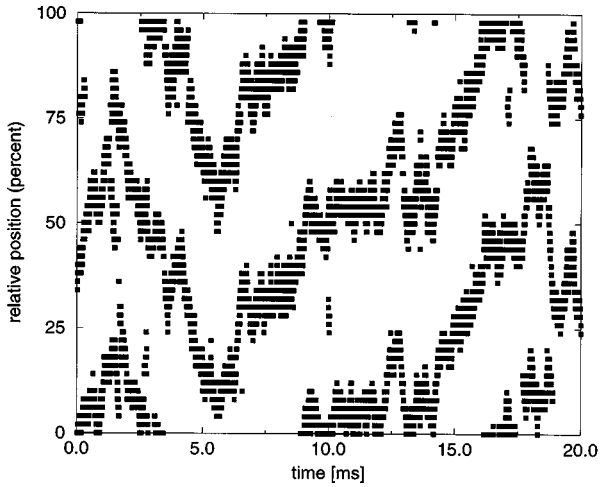

FIG. 2. Positions of end loops of a 1475-bp DNA structure ($\Delta Lk=-8$, $0.1M$ NaCl) versus simulation time.

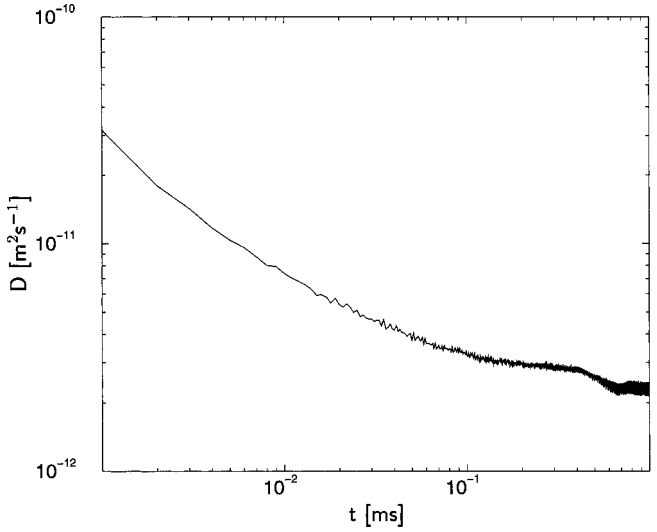

FIG. 3. Diffusive motion of the two strands of the superhelix (slithering) of a 1475-bp DNA structure ($\Delta Lk=-8$, 0.1M NaCl). The diffusion coefficient $D_{sl}=\langle x^2\rangle/2t$ is plotted against t.

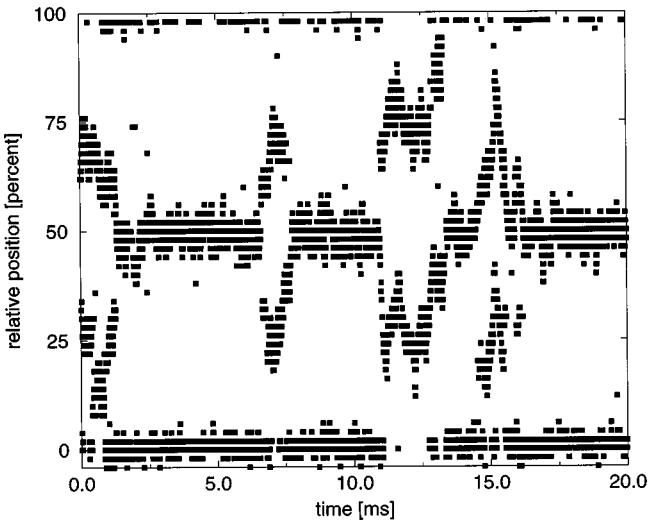

FIG. 5. Positions of end loops of 1475-bp DNA, $\Delta Lk=-8$, 0.1M NaCl, with a permanent bend at 0% of the length, plotted against simulation time.

branched states to $5.7/18.5\approx 0.3$, which is about 3 times higher than without the bend.

Systems that differ in length (1180–1770 bp), linking number (-6 to -8), and ionic strength ($0.01M-1M$ NaCl) from the previous system were calculated for 5 ms, each with a permanent bend of 90°. We confirmed the previous observation of this and other groups that in these systems DNA has a linear plectonemic structure with the bend in an end loop [7,21]. Corresponding superhelix diameters are summarized in Table II. The errors of 1475-bp DNA, $\Delta Lk=-8$ at $I=0.1M$, are smaller because, due to a longer simulation time, the data basis is bigger. In solution of an ionic strength of 0.01M the simulation time step had to be decreased by a factor of 4–5 ns. With this time step it was not possible to collect enough data in reasonable time so that we decided not to examine the end loop dynamics of superhelical DNA under these conditions.

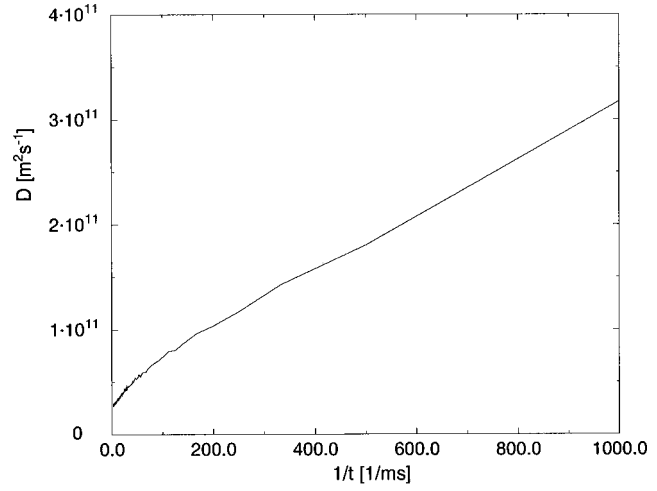

FIG. 4. Diffusive motion of the two strands of the superhelix (slithering) of a 1475-bp DNA structure ($\Delta Lk=-8$, 0.1M NaCl). The diffusion coefficient D_{sl} is plotted against $1/t$.

B. Nonequilibrium

As we have seen in Sec. III A, the most probable configuration for the superhelical DNA considered here is unbranched and has the permanent bend at one end loop. If we put a new permanent bend into a configuration of a nonbent DNA structure, we expect this permanent bend to move to the end loop. To assess the relaxation time for this process we first equilibrate the starting configuration with a permanent bend at position 0, change the position of the permanent bend to another location, and continue the simulation until equilibrium is reached again.

There are two possible mechanisms to explain the restructuring: The two strands are moving relative to each other (slithering) until the permanent bend has reached one end loop and is trapped there, or a new arm is formed and grows until one of the initial arms disappears [8]. We observed both mechanisms: In Fig. 6 we see end loop plots of two different simulations, each one exhibiting one type of restructuring.

Since both slithering and rearrangement of arms occur in a random, nondirected way, one would expect a dependence of the relaxation time on the distance between the bend and the end loop. We have performed simulations of a 1475-bp DNA structure with $\Delta Lk=-8$ at an ionic strength of 0.1M NaCl and determined the relaxation time as a function of this distance. The mean values of the relaxation times of ten calculations for each distance are shown in Fig. 7. The relaxation times show a broad distribution around the mean value. The overall mean value is (0.64 ± 1.07) ms, but a clear maximum is seen if the bend is inserted in the center.

Figure 8 shows the mean relaxation times after inserting a permanent bend at a distance of 80 nm (236 bp) from the end loop for lengths between 1180 and 1770 bp. The other parameters (superhelix density and ionic strength) remain unchanged. For each length we performed eight simulations. The mean relaxation times after inserting a permanent bend at the same distance for superhelix densities between -0.043 and -0.057 are shown in Fig. 9. The relaxation time under these conditions at 0.1M NaCl is (0.64 ± 0.29) ms, at 1M (1.61 ± 1.63) ms.

TABLE II. Mean value and standard deviation of the superhelix diameter dependent on physical parameters. If not mentioned differently, the length is 1475 bp, the superhelix density is -0.057, and the ionic strength is 0.1*M* NaCl.

Length (bp)	d_{SH} (nm)	Ionic strength (*M* NaCl)	d_{SH} (nm)	Superhelix density	d_{SH} (nm)
1180	9.1±1.9			−0.057	10.4±1.0
1475	10.4±1.0	0.1	10.4±1.0	−0.050	13.2±2.8
1770	10.9±1.7	1	8.7±1.4	−0.043	15.3±3.7

IV. DISCUSSION

A. Equilibrium

According to Tirado and Garcia de la Torre [22,23], the diffusion coefficient of a cylinder with length l and hydrodynamic radius r_{HD} is

$$D^{cyl}=(1/3)(D_{\parallel}^{cyl}+2D_{\perp}^{cyl}), \tag{11}$$

with

$$D_{\parallel}^{cyl}=\frac{k_BT}{2\pi\eta l}(\ln p-0.207+0.980p^{-1}-0.133p^{-2}),$$
$$D_{\perp}^{cyl}=\frac{k_BT}{4\pi\eta l}(\ln p-0.839+0.185p^{-1}+0.233p^{-2}), \tag{12}$$

$$p=\frac{l}{2r_{HD}}, \tag{13}$$

where η is the viscosity of the solvent and T its temperature. For a rod of length 50 nm (147 bp) and a hydrodynamic radius 1.2 nm, Eq. (11) yields 2.89×10^{-11} m^2/s. The persistence length of DNA is 50 nm, therefore we considered this fragment stiff in a first approximation. The value computed by Brownian dynamics [$(2.85\pm0.01)\times10^{-11}$ m^2/s] agrees with the rigid rod value within statistical error. Experimental sedimentation velocity studies of double stranded DNA fragments of 145-bp DNA yield a sedimentation coefficient $s^0_{20,w}$ of 5.2 [24]. This is equivalent to a diffusion coefficient of 2.7×10^{-11} m^2/s, again in good agreement with our computation.

Monte Carlo calculations of equilibrium configurations of superhelical DNA were done by Vologodskii *et al.* [21]. With the results presented there it is possible to calculate the ratio of conformations with three arms (without permanent bends). For DNA of 1475 bp and superhelix density -0.057, their equations predict a ratio of 0.03, which is about 4 times smaller than our value for DNA without permanent bends. Our value is more approximate because the trajectory is too

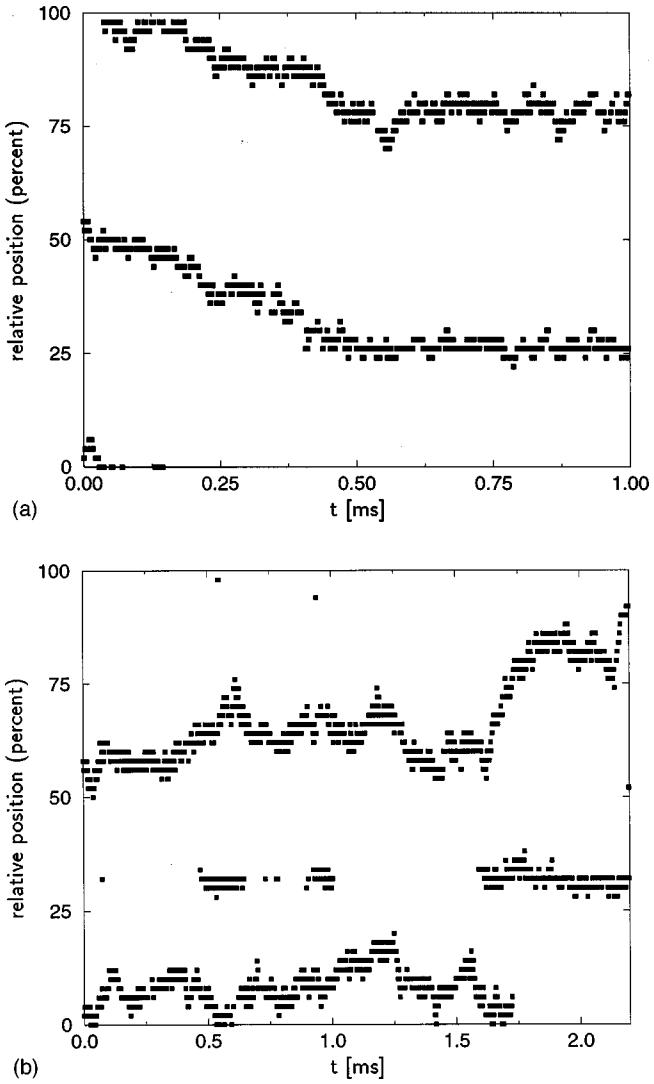

FIG. 6. Positions of end loops plotted against simulation time after inserting a permanent bend (a) at 26% of length showing slithering and (b) at 32% showing structural rearrangement.

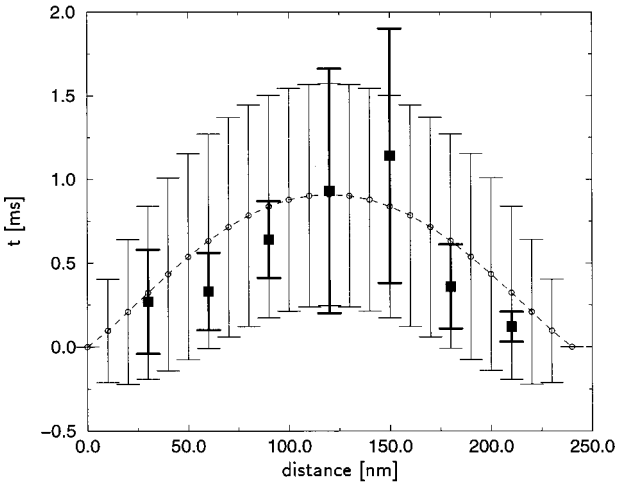

FIG. 7. Relaxation time for different distances of the inserted permanent bend to the end of the superhelix. Data are from simulations (bold squares) and the simplified model (circles).

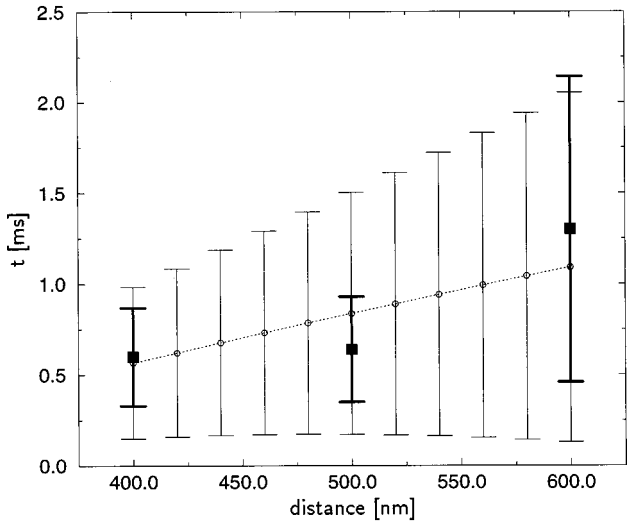

FIG. 8. Relaxation time after inserting a permanent bend for different lengths of DNA. The data from simulations (squares with bold error bars) are compared with the simplified model (circles).

short for an exact determination of this value. This can be seen, e.g., from the fact that we observed only one short time period of three-arm configurations. Nevertheless, both values are of the same order of magnitude.

A comparison of Fig. 2 with Fig. 5 suggests that this ratio is bigger for DNA with a permanent bend. This is in agreement with results of simulations by Sprous and Harvey [25]. Klenin *et al.* [7] report a ratio of 0.25 of branched states for 2700-bp DNA with and without a permanent bend. This might suggest that a permanent bend has less influence on the global structure of longer DNA. All studies predict that permanent bends are located at an end loop with high probability.

Questions similar to those in Sec. III A were analyzed by Sprous and Harvey on a 1260-bp DNA structure with a model based on molecular dynamics [25]. Their end loop plots look similar to those presented here. In their calculations a superhelix without a bent sequence is always unbranched. Our calculations disagree with their observation that DNA with a bend is mostly branched.

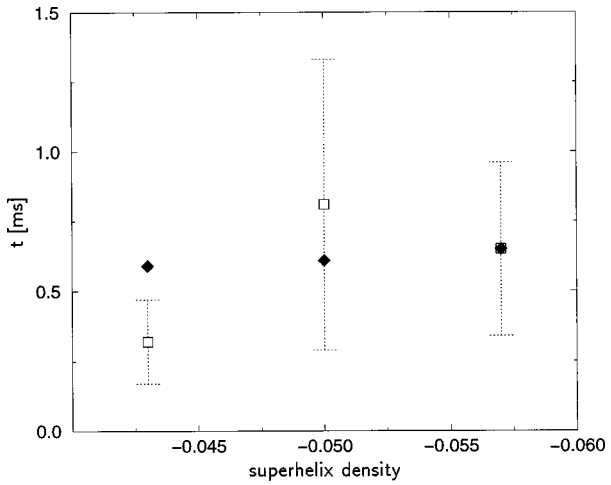

FIG. 9. Relaxation time after inserting a permanent bend for different superhelix densities. The data from simulation (squares with error bars) are compared with predicted values according to Eq. (15) (diamonds).

TABLE III. Comparison of the values of the superhelix diameter (nm) measured by Boles *et al.* and our results.

Superhelix density	Experiment	Theory
-0.057	11.9	10.4 ± 1.0
-0.050	13.4	13.2 ± 2.8
-0.043	15.3	15.3 ± 3.7

We find that the slithering diffusion coefficient of a 1475-bp DNA structure at short time scales is 31.7×10^{-12} m^2/s. This is in agreement with the value of 30×10^{-12} m^2/s calculated by Chirico and Langowski analyzing the motion of one segment tangent to the chain [8]. The diffusion coefficient for larger time scales decreases to $(2.5\pm0.2)\times10^{-12}$ m^2/s; this smaller value corresponds to the correlated slithering of the whole chain.

Superhelix diameters for different superhelix densities determined by electron microscopical methods [26] are in good agreement with the values calculated here (Table III). The measured and the theoretical values agree within 5%, which is smaller than the error of about 1 nm of the theoretical and experimental values. It is notable, however, that all three theoretical values are bigger than the measured ones. The reason could be the procedure of analysis of the experimental data. Boles *et al.* also report about another more approximate procedure of analysis whose results are about 1 nm bigger. However, they examined DNA fixed on a surface and we investigate free DNA in solution.

Recent scanning force microscope measurements of 1868-bp superhelical DNA [27] gave an average superhelical diameter of 27 ± 9 nm at a superhelix density of $\sigma=-0.033$. This is comparable to the trend of our results.

B. Nonequilibrium

A smaller set of nonequilibrium states of 1870-bp DNA ($\Delta Lk=-10$) was analyzed by Chirico and Langowski [8]. By analyzing trajectories up to 2 ms they concluded that large-scale changes of conformation are mainly caused by the rearrangement of branches rather than slithering. This analysis with about 40 times more data now implies that slithering is another important mechanism of restructuring. For a detailed analysis of the dependence between the slithering diffusion coefficient and the restructuring time see Sec. IV C.

Tan *et al.* investigated shorter DNA (600 bp) using molecular dynamics simulations without hydrodynamic interactions [20]. They found that at higher superhelix density the structural changes are mainly caused by slithering while at lower superhelix density structural rearrangements become more important. This conclusion may not be valid for larger DNA structures, 600 bp being equal to about only four persistence lengths. The calculated relaxation time is of the order of nanoseconds, about six orders of magnitude faster than in calculations using Brownian dynamics such as [8] and our investigations. The cause of this difference is the lack of stochastic forces and hydrodynamic friction in the

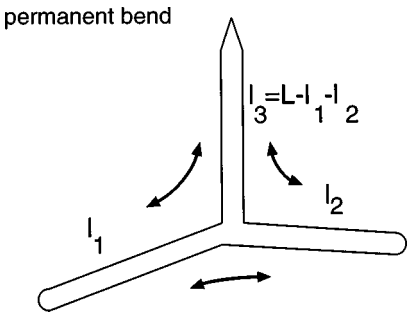

FIG. 10. Model of DNA that consists of three loops that change their lengths in a diffusive manner. The double arrows symbolize the possible transitions. The permanent bend is located at the tip of loop 3.

thermal molecular dynamics model.

A possible explanation of the different relaxation times at different superhelix densities is proposed by Marko and Siggia [28]. From the diffusive motion of two parallel cylinders along their long axis they estimate a typical time for a diffusive slithering motion of superhelical DNA:

$$\tau_s = \frac{2\pi\eta L^3}{k_B T \ln(R/r_h)}. \tag{14}$$

η is the viscosity of water, $2L$ the length of the DNA, r_h the hydrodynamic radius of the DNA, and R the superhelix radius. While τ_s scales with L^3, the relaxation times we observed scale with L^2 [Eq. (9)]. The other scaling behavior reflects that DNA is not stiff. It can be thought of as consisting of smaller parts that move independently, changing their distance to each other. A detailed analysis has been done recently by Marko [29]. As an approximation we can assume that the time scales of the motion of the smaller parts scale with superhelix diameter in the same way as τ_s and therefore estimate the relaxation time at different superhelical densities. Equation (14) can be written as

$$\frac{\tau_s^{(1)}}{\tau_s^{(2)}} = \frac{\ln(R_2/r_h)}{\ln(R_1/r_h)}. \tag{15}$$

Starting from the relaxation time at $\sigma = -0.057$ and the calculated superhelix diameter (Table II), we determine the relaxation times at other superhelix densities (Fig. 9). The results seem to be compatible with the values obtained from the simulation.

C. Simplified numerical model

In order to get an estimate of the scaling of the relaxation times as a function of different parameters such as length or position of inserted bend we developed a simplified model that allows us to get these times with much less computational effort. The model consists of three arms with varying discrete numbers of segments (see Fig. 10). One move consists of a segment interchange between the arms with the lengths l_1, l_2, l_3. We assume that the influence of the probability for each of these moves on the configuration can be neglected. The permanent bend is always at the tip of arm 3. This excludes branched states where the bend is not in an end loop. The total length remains constant and therefore the system can be described by the lengths of two arms. The system is moving in a two-dimensional state space. At each step there are six different possible transitions for branched and four for unbranched states. In our model the equilibrium, where the bend is in an end loop and no branches are present, has the property

$$l_1 = 0 \vee l_2 = 0. \tag{16}$$

The changes of the lengths can be described as a random walk on a directed weighted graph. The vertices of the graph represent possible states and the edges possible transitions. Each vertex has a certain probability of being occupied at each time step. For the next time step the new probability of a vertex being occupied is given by the probability of the neighbor vertices weighted by the probabilities of transition, i.e., the weights of the edges.

The probability of a state with arm lengths l_1 and l_2 after p steps can be described using a (normalized) probability matrix $\Psi_p(l_1, l_2)$:

$$\sum_{l_1, l_2 = 0}^{L} \Psi_p(l_1, l_2) = 1. \tag{17}$$

The sums of the probabilities at the vertices fulfilling condition (16) give the probability that the system has reached an equilibrium state in this step. The probability that the equilibrium states are reached after p steps is then

$$\sum_{\lambda=0}^{L} \Psi_p(0,\lambda) + \sum_{\lambda=0}^{L} \Psi_p(\lambda,0). \tag{18}$$

The state after each time step can be calculated using a transfer matrix T:

$$\Psi_{p+1} = T\Psi_p. \tag{19}$$

$T_{(l_1,l_2)(l_1',l_2')}$ is the probability for the transition from state $\{l_1, l_2\}$ to $\{l_1', l_2'\}$. For equilibrium states we have $T_{(l_1,l_2)(l_1,l_2)} = 1$ and zero for transitions to other states. For nonequilibrium $\{l_1, l_2\}$ only six transitions are possible (arrows in Fig. 10). This means that then $T_{(l_1,l_2)(l_1',l_2')}$ is zero except in the cases

$$\begin{aligned} l_1 - l_1' &= \pm 1 \wedge l_2 - l_2' = 0, \\ l_2 - l_2' &= \pm 1 \wedge l_1 - l_1' = 0, \\ l_1 - l_1' &= \pm 1 \wedge l_2 - l_2' = \mp 1. \end{aligned} \tag{20}$$

The probability that a state with two arms changes into a state with three arms is expressed by the branching probability w_{branch}. Thus the elements of $T_{(l_1,l_2)(l_1',l_2')}$ can be written for nonequilibrium $\{l_1, l_2\}$ as

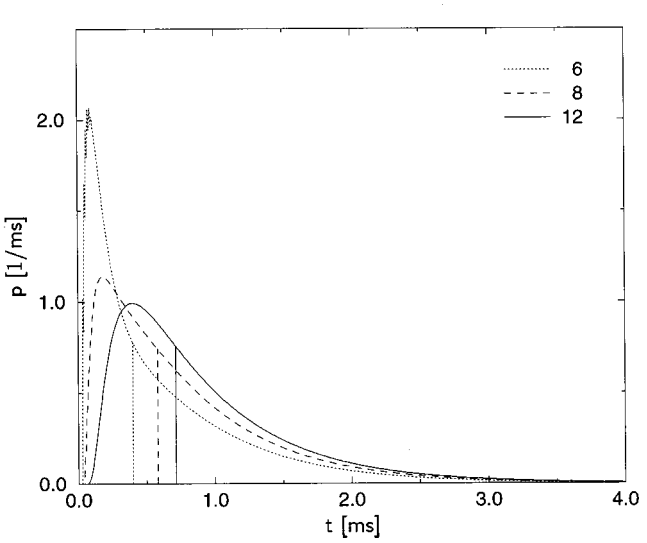

FIG. 11. Probability density of the relaxation times for the distances 6, 8, and 12 segments of 50 segments of the permanent bend to the end of the superhelix. The times at which the total probability has reached 50% are marked with vertical lines.

$$T_{(l_1,l_2)(l_1',l_2')}=\begin{cases}1/6, & l_1+l_2<L\wedge l_1'+l_2'\leqslant L\\ 0{,}5-w_{branch}/2, & l_1+l_2=L\wedge l_1'+l_2'=L\\ w_{branch}/2, & l_1+l_2=L\wedge l_1'+l_2'<L\\ 0, & \text{in all other cases.}\end{cases} \tag{21}$$

Starting from one special configuration Ψ_0, we can compute the probability matrices Ψ_p; $p>0$ iteratively using Eq. (19). The probability to reach equilibrium is given by Eq. (18). From this distribution of the relaxation time we can compute the mean and variance.

The relation between a model step and a real time step is not given *a priori* and one has to calibrate the time scale

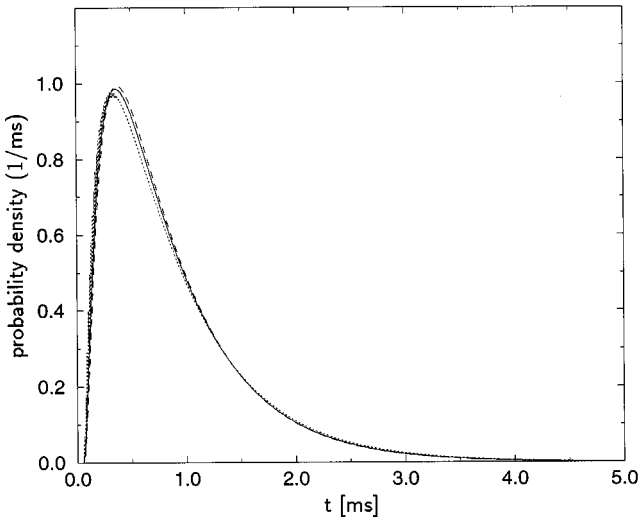

FIG. 12. Distribution of the relaxation times after inserting a permanent bend at a distance 9 segments away from the end of the superhelix in a chain of 50 segments for branching probabilities of 1 (dashed line), 0.5 (solid line), and 0.02 (dotted line).

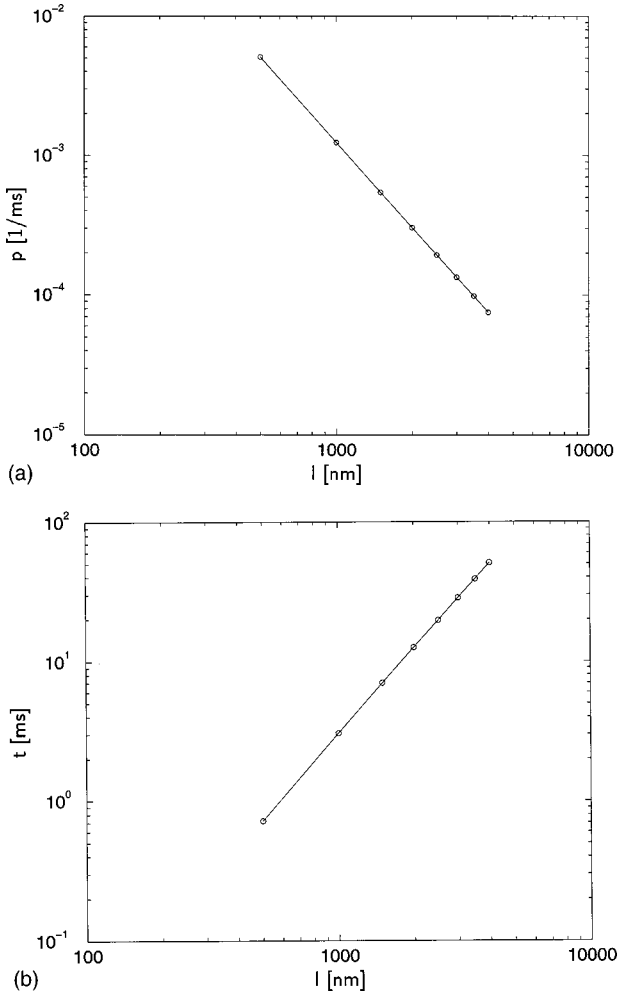

FIG. 13. Finite size scaling for different sizes of the system. The permanent bend is inserted in the middle between the ends of the superhelix. The abscissa shows the length of the DNA L and the ordinate (a) the probability density at 50% total probability and (b) the time at this probability. The relaxation time is proportional to $L^{-2,03}$ and the probability density is proportional to $L^{2,045}$.

against the BD simulation. For that reason we compared the relaxation times for different distances between the inserted permanent bend and the end of the superhelix from the simulation and the times predicted by the model (see Fig. 7). Using a Gaussian least-squares method we found that the value 1 ms/145.7=6.9 μs per step in the model minimized the difference between the simulation and model. With this value we calibrated the calculations of the model for different lengths of DNA and compared it with the results from the BD simulations (Fig. 8) with good agreement.

The mean time of the diffusive motion of a segment by its own length in BD simulations can be computed using the slithering diffusion coefficient and Eq. (10) to 20 μs of the same order as the calibration value. Therefore, it is possible to describe the dependence of the relaxation time on the distance of the permanent bend from the end of the superhelix and on the length of the DNA by a simplified numerical model without adjusting parameters such as the branching probability. This model also allows one to calculate larger systems with more branches; the state space will then have a higher dimension.

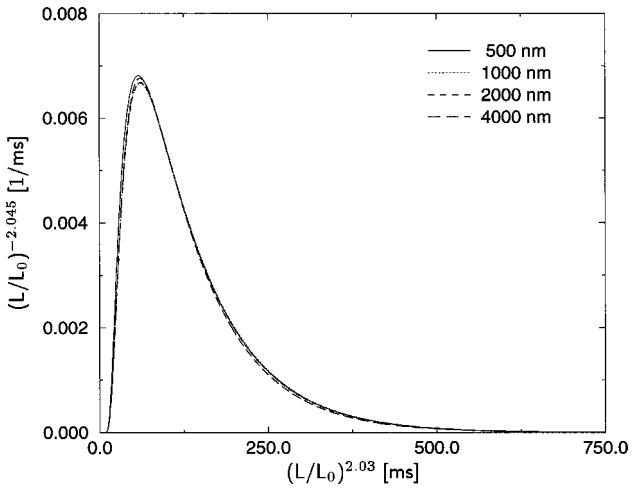

FIG. 14. Scaling plot of the relaxation times of DNA of the lengths 500, 1000, 2000, and 4000 nm with $L_0 = 500$ nm.

The probability density that the system is in equilibrium after inserting a permanent bend is shown in Fig. 11 for different distances from the end of the superhelix. The distribution is quite skewed with a long tail to high t values; the time when the system has reached the equilibrium with 50% probability is much larger than the time at the maximum. The BD results tentatively show the same behavior (Sec. III B).

The probability densities for different branching probabilities are shown in Fig. 12. Despite the difference of a factor of 50 in the branching probability there is hardly a change. Thus, in this model the branching probability has almost no influence.

We then analyzed the scaling of the distribution of the relaxation time by choosing the time at which the probability P for reaching equilibrium is 50% and the probability at this point. These two values were determined at different lengths for inserting a permanent bend in the middle between the ends of the superhelix, i.e., the maximal distance (Fig. 13). Regression with a power law shows that the relaxation time scales as $L^{-2.03}$ and the probability density scales as $L^{2.04}$. Extrapolation to infinite length gives exponents of -2.01 ± 0.01 and 2.02 ± 0.01, respectively. Using the master curve, one can compute the distribution for all other lengths [30]. Figure 14 shows four distributions plotted according to the scaling law

$$P_L(t) = \left(\frac{\tilde{L}}{L}\right)^{2.04} \tilde{P}_{\tilde{L}}\left[\left(\frac{\tilde{L}}{L}\right)^{-2.03} t\right]. \tag{22}$$

Only minor deviations from this scaling are visible. For much longer DNA states with three arms will be part of the equilibrium distribution and states with four arms get significant weights.

V. CONCLUSION

In this work we computed the time scales of structural changes of superhelical DNA induced by bending using computer simulations based on a Brownian dynamics model. We focused on circular, superhelical 1475-bp DNA with a superhelix density of -0.057, which is approximately the *in vivo* value, for a solution of physiologic ionic strength. We confirmed previously reported results that in the equilibrium state DNA has the shape of an unbranched superhelix. Without a bend the two double strands are moving diffusively against each other with a diffusion constant of $(2.5 \pm 0.2) \times 10^{-12}$ m^2/s.

After insertions of a permanent bend of 90° the system relaxed to a state with the bend in an end loop. The relaxation proceeds by two different mechanisms: a slithering motion of the two double strands and restructuring due to formation of arms. The relaxation time after inserting a permanent bend was computed for different distances between the inserted permanent bend and the end of the superhelix. The mean value is (0.64 ± 1.07) ms; the maximum time when the bend is inserted in the center of the plectonemic structure is (1.0 ± 0.7) ms. At an ionic strength of 1M NaCl the relaxation time is about 2.5 times greater than at 0.1M. The calculated times for different superhelix densities differs only in the range of the errors, in agreement with previous analytical estimates.

Because the distribution of the relaxation time is quite skewed and has a long tail it is difficult to obtain results with reasonable statistics. On different supercomputers we had to calculate about 500 ms of trajectory time equivalent to a CPU time of about 5 yr on an IBM RS 6000 Power 2.

We showed that it is possible to describe the dependences of the relaxation time on the distances of the inserted permanent bend to the end of the superhelix and on the length of the DNA by a simplified numerical model based on a random walk on a graph. The relaxation time scales with the square of the DNA length. For longer DNA more branches are probable; then the model would require one to increase the dimension of the state space. The computed values of the relaxation time are in the range of the reaction times of enzymatic reactions, which means that the kinetics of binding of DNA-bending proteins can influence transcriptional regulation.

ACKNOWLEDGMENTS

This work was supported by a grant from the German Scholarship Foundation to Gero Wedemann and by BMBF Grant No. 01 KW 9620 (German Human Genome Project DHGP).

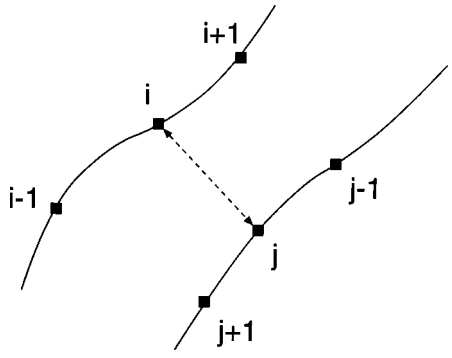

FIG. 15. Definition of the plectonemic region. Segments i and j are nearest neighbors.

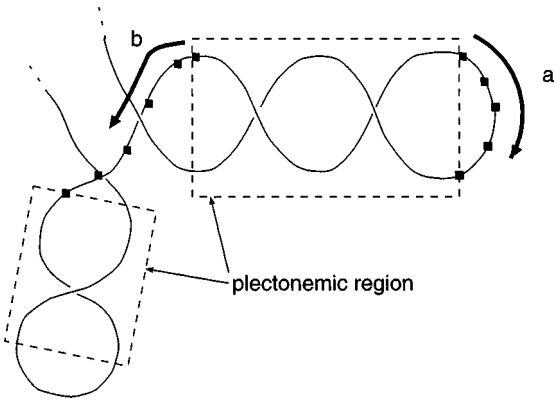

FIG. 16. Decision whether the end of a plectonemic region is an end loop. Following direction *a*, we go back to the same region, so it is an end loop. Following direction *b*, we reach another plectonemic region, so it cannot be an end loop.

APPENDIX: ALGORITHM FOR END LOOP DETECTION

The basis for the end loop detection is the notion of the plectonemic region [8]. A plectonemic region is defined as a part of the DNA where the two double strands are wound around each other in opposite directions. We define the function $nb(i,j)$ to be true if segment j is the next nearest neighbor to segment i; otherwise it is false. A segment i is defined as part of a plectonemic region if $nb(i,j(i))$, $nb(i-1,j(i)+1)$, and $nb(i+1,j(i)-1)$ are true *or* if $nb(i,j(i))$, $nb(i-1,j(i)+1+k)$, and $nb(i+1,j(i)-1+l)$, $l,k\in\{-1,0,+1\}$, are true (see Fig. 15) and the angles between the segment and its nearest neighbor are less than $\phi_{plect}=30°$.

After assigning all plectonemic segments we identify successive plectonemic segments and their nearest neighbors. If a plectonemic region follows at the end of another one, the first region cannot be terminated by an end loop. In the case of an end loop the region would be reached again after S segments (see Fig. 16). If $S\leqslant N_{nonwrithed}=11$ or $S\leqslant N_{writhed}=15$ and $w(j)\leqslant 0.5$ with

$$w(j)=\frac{1}{2\pi}\int_{r_{j-q}}^{r_j}\int_{r_{j+1}}^{r_{j+q+1}}\frac{(d\vec{r}_1\times d\vec{r}_2)\cdot\vec{r}_{1,2}}{|\vec{r}_{1,2}|^3} \qquad \text{(A1)}$$

there is an end loop at this end of the region. The integral in Eq. (A1) is a measure for the number of strand crossovers in projections. Recently, it was possible to enhance the acceptance rate to 99% by using an exact expression for the integral in Eq. (A1) instead of an approximating sum [8].

[1] K. Rippe, P. H. von Hippel, and J. Langowski, Trends Biochem. Sci. **20**, 500 (1995).
[2] J. Langowski, in *Nucleic Acids and Molecular Biology*, edited by D. Lilley and F. Eckstein (Springer, Heidelberg, 1997), Vol. 11, pp. 219–235.
[3] H. Merlitz, K. Rippe, K. Klenin, and J. Langowski, Biophys. J. **74**, 773 (1998).
[4] K. Klenin, H. Merlitz, and J. Langowski, Biophys. J. **74**, 780 (1998).
[5] C. Laundon and J. Griffith, Cell **52**, 545 (1988).
[6] C. Pfannschmidt and J. Langowski, J. Mol. Biol. **275**, 601 (1998).
[7] K. Klenin, M. Frank-Kamenetskii, and J. Langowski, Biophys. J. **68**, 81 (1995).
[8] G. Chirico and J. Langowski, Biophys. J. **71**, 955 (1996).
[9] T. Schlick, Curr. Opin. Struct. Biol. **5**, 245 (1995).
[10] D. Ermak and J. McCammon, J. Chem. Phys. **69**, 1352 (1978).
[11] R. Tan and S. Harvey, J. Mol. Biol. **205**, 573 (1989).
[12] T. Schlick and W. Olson, J. Mol. Biol. **223**, 1089 (1992).
[13] M. Fixman, J. Chem. Phys. **69**, 1527 (1978).
[14] S. Allison, R. Austin, and M. Hogan, J. Chem. Phys. **90**, 3843 (1989).
[15] G. Chirico and J. Langowski, Biopolymers **34**, 415 (1994).
[16] D. Stigter, Biopolymers **16**, 1435 (1977).
[17] J. Rotne and S. Prager, J. Chem. Phys. **50**, 4831 (1969).
[18] S. Smith, Y. Cui, and C. Bustamante, Science **271**, 795 (1996).
[19] M. Hammermann, Diploma thesis, University of Heidelberg, 1996 (unpublished).
[20] R. Tan, D. Sprous, and S. Harvey, Biopolymers **39**, 259 (1996).
[21] A. Vologodskii *et al.*, J. Mol. Biol. **227**, 1224 (1992).
[22] M. Tirado and J. Garcia de la Torre, J. Chem. Phys. **71**, 2581 (1979).
[23] M. Tirado and J. Garcia de la Torre, J. Chem. Phys. **73**, 1986 (1980).
[24] R. T. Kovacic and K. E. van Holde, Biochemistry **16**, 1490 (1977).
[25] D. Sprous and S. Harvey, Biophys. J. **70**, 1893 (1996).
[26] C. Boles, J. White, and N. Cozzarelli, J. Mol. Biol. **213**, 931 (1990).
[27] K. Rippe, N. Mücke, and J. Langowski, Nucleic Acids Res. **25**, 1736 (1997).
[28] J. F. Marko and E. D. Siggia, Phys. Rev. E **52**, 2912 (1995).
[29] J. F. Marko, Physica A **244**, 263 (1997).
[30] K. Binder and D. Heermann, *Monte Carlo Simulation in Statistical Physics*, 2nd ed. (Springer, Berlin, 1992).